GEOARCHAEOLOGICAL XRF LAB
A GREEN SOLAR FACILITY

GEOARCHAEOLOGICAL X-RAY FLUORESCENCE SPECTROMETRY LABORATORY
8100 Wyoming Blvd., Ste M4-158 Albuquerque, NM 87113
USA

ENERGY-DISPERSIVE X-RAY FLUORESCENCE (EDXRF) WHOLE ROCK ANALYSIS OF MAJOR, MINOR AND TRACE ELEMENTS FOR OBSIDIAN AND OTHER VOLCANIC ROCK ARTIFACTS FROM THE EL SEGUNDO ARCHAEOLOGY PROJECT, NORTHWESTERN NEW MEXICO

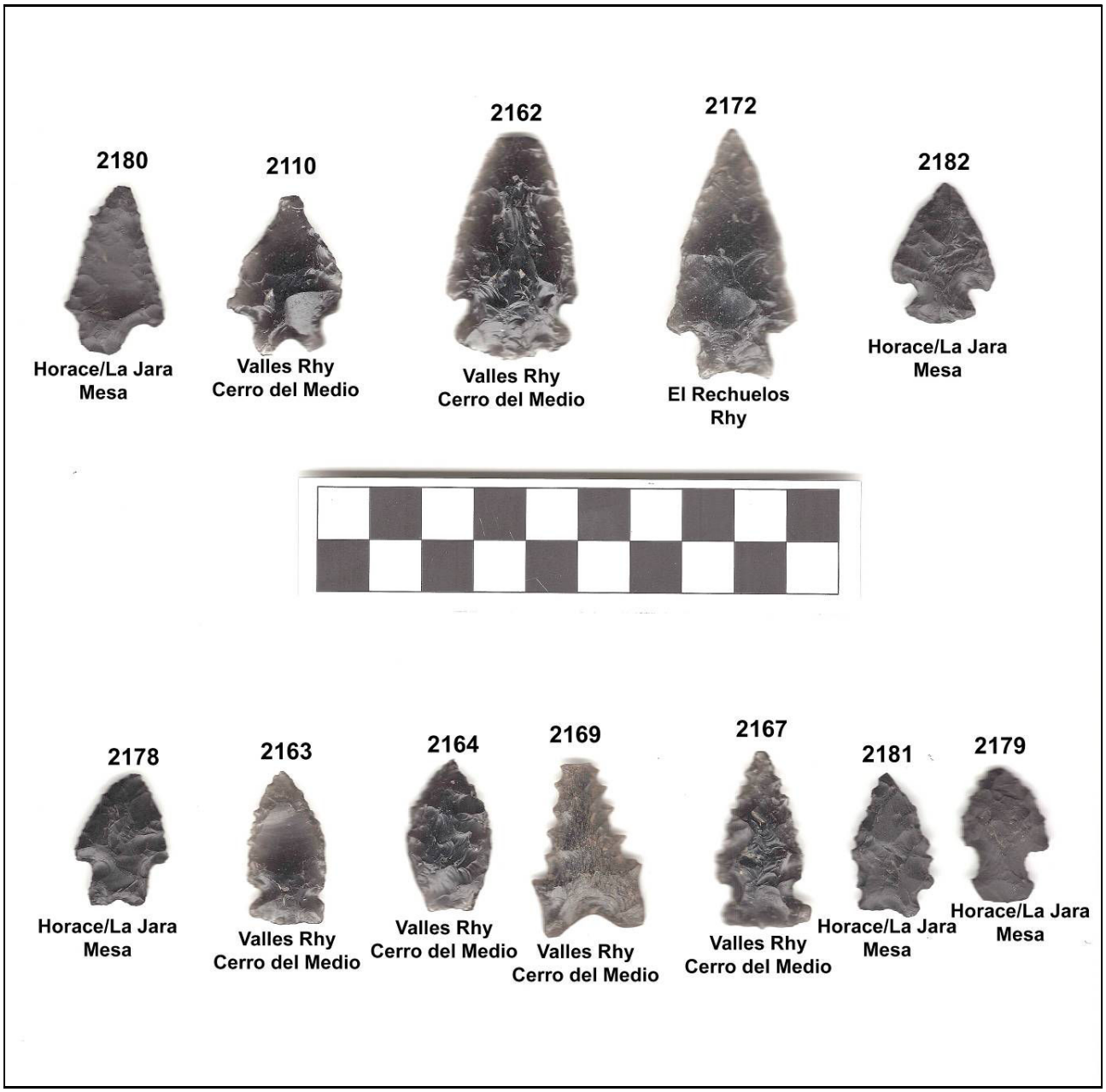

Selected obsidian Archaic projectile points from the project area.

ENERGY-DISPERSIVE X-RAY FLOURESCENCE (EDXRF) WHOLE ROCK ANALYSIS OF MAJOR, MINOR AND TRACE ELEMENTS FOR OBSIDIAN AND OTHER VOLCANIC ROCK ARTIFACTS FROM THE EL SEGUNDO ARCHAEOLOGY PROJECT, NORTHWESTERN NEW MEXICO

by

M. Steven Shackley, Ph.D., Director
Geoarchaeological XRF Laboratory
Albuquerque, New Mexico

Report Prepared for

Steven Mack, Project Manager
Southwest Archaeological Consultants
Santa Fe, New Mexico

14 December 2018

INTRODUCTION

The analysis here of a variety of artifacts from a number of sites or site groups in the El Segundo project area is dominated by obsidian sources along the Jemez Lineament, and a variety of rock types likely typical of the local geology. One piece of obsidian debitage was produced from the Government Mountain source in the San Francisco Volcanic Field or northern Arizona, over 370 linear km west. Government Mountain obsidian has occurred in El Segundo project sites and other Archaic contexts in the Grants, New Mexico area just south of El Segundo (Birkmann et al. 2018). One dacite projectile point base was produced from the San Antonio Mountain source in the Taos Plateau Volcanic field over 250 linear km north. These results are similar to previous studies of sites in the area, and support the provenance inferences from these studies (see Birkmann et al. 2018; Shackley 2015a, 2015b, 2016, 2017). The results here indicate that a future reconnaissance, and sampling of local volcanic rocks could be fruitful for archaeological interpretation.

LABORATORY SAMPLING, ANALYSIS AND INSTRUMENTATION

All archaeological samples are analyzed whole. The results presented here are quantitative in that they are derived from "filtered" intensity values ratioed to the appropriate x-ray continuum regions through a least squares fitting formula rather than plotting the proportions of the net intensities in a ternary system (McCarthy and Schamber 1981; Schamber 1977). Or more essentially, these data through the analysis of international rock standards, allow for inter-instrument comparison with a predictable degree of certainty (Hampel 1984; Shackley 2011b).

All analyses for this study were conducted on a ThermoScientific *Quant'X* EDXRF spectrometer, located at the Geoarchaeological XRF Laboratory, Albuquerque, New Mexico. It is equipped with a thermoelectrically Peltier cooled solid-state Si(Li) X-ray detector, with a 50

kV, 50 W, ultra-high-flux end window bremsstrahlung, Rh target X-ray tube and a 76 μm (3 mil) beryllium (Be) window (air cooled), that runs on a power supply operating from 4-50 kV/0.02-1.0 mA at 0.02 increments. The spectrometer is equipped with a 200 l min^{-1} Edwards vacuum pump, allowing for the analysis of lower-atomic-weight elements between sodium (Na) and titanium (Ti). Data acquisition is accomplished with a pulse processor and an analogue-to-digital converter. Elemental composition is identified with digital filter background removal, least squares empirical peak deconvolution, gross peak intensities and net peak intensities above background.

Trace Element Analysis

The analysis for mid Zb condition elements Ti-Nb, Pb, Th, the x-ray tube is operated at 30 kV, using a 0.05 mm (medium) Pd primary beam filter in an air path at 100 seconds livetime to generate x-ray intensity $K\alpha_1$-line data for elements titanium (Ti), manganese (Mn), iron (as $Fe_2O_3^T$), cobalt (Co), nickel (Ni), copper, (Cu), zinc, (Zn), gallium (Ga), rubidium (Rb), strontium (Sr), yttrium (Y), zirconium (Zr), niobium (Nb), lead (Pb), and thorium (Th). Not all these elements are reported since their values in many volcanic rocks are very low. Trace element intensities were converted to concentration estimates by employing a linear calibration line ratioed to the Compton scatter established for each element from the analysis of international rock standards certified by the National Institute of Standards and Technology (NIST), the US. Geological Survey (USGS), Canadian Centre for Mineral and Energy Technology, and the Centre de Recherches Pétrographiques et Géochimiques in France (Govindaraju 1994). Line fitting is linear (XML) for all elements. When barium (Ba) is analyzed in the High Zb condition, the Rh tube is operated at 50 kV and up to 1.0 mA, ratioed to the bremsstrahlung region (see Davis 2011; Shackley 2011b). Further details concerning the petrological choice of these elements in Southwest obsidians is available in Shackley (1988,

1995, 2005; also Mahood and Stimac 1991; and Hughes and Smith 1993). Nineteen specific pressed powder standards are used for the best fit regression calibration for elements Ti-Nb, Pb, Th, and Ba, and include G-2 (basalt), AGV-2 (andesite), GSP-2 (granodiorite), SY-2 (syenite), BHVO-2 (hawaiite), STM-1 (syenite), QLO-1 (quartz latite), RGM-1 (obsidian), W-2 (diabase), BIR-1 (basalt), SDC-1 (mica schist), TLM-1 (tonalite), SCO-1 (shale), NOD-A-1 and NOD-P-1 (manganese) all US Geological Survey standards, NIST-278 (obsidian), U.S. National Institute of Standards and Technology, BE-N (basalt) from the Centre de Recherches Pétrographiques et Géochimiques in France, and JR-1 and JR-2 (obsidian) from the Geological Survey of Japan (Govindaraju 1994).

Major and Minor Oxide Analysis

Analysis of the major oxides of Si, Al, Ca, Fe, K, Mg, Mn, Na, and Ti is performed under the multiple conditions elucidated below. This fundamental parameter analysis (theoretical with standards), while not as accurate as destructive analyses (pressed powder and fusion disks) is usually within a few percent of actual, based on the analysis of USGS RGM-1 obsidian or in this study the USGS AGV-1 andesite standard (see also Shackley 2011b). The fundamental parameters (theoretical) method is run under conditions commensurate with the elements of interest and calibrated with 11 USGS standards (RGM-1, rhyolite; AGV-2, andesite; BHVO-1, hawaiite; BIR-1, basalt; G-2, granite; GSP-2, granodiorite; BCR-2, basalt; W-2, diabase; QLO-1, quartz latite; STM-1, syenite), and one Japanese Geological Survey rhyolite standard (JR-1). See Lundblad et al. (2011) for another set of conditions and methods for oxide analyses.

Conditions Of Fundamental Parameter Analysis[1]:

Low Za (Na, Mg, Al, Si, P)

Voltage	6 kV	Current	Auto[2]
Livetime	100 seconds	Counts Limit	0

Filter	No Filter	Atmosphere	Vacuum
Maximum Energy	10 keV	Count Rate	Low

Mid Zb (K, Ca, Ti, V, Cr, Mn, Fe)

Voltage	32 kV	Current	Auto
Livetime	100 seconds	Counts Limit	0
Filter	Pd (0.06 mm)	Atmosphere	Vacuum
Maximum Energy	40 keV	Count Rate	Medium

High Zb (Sn, Sb, Ba, Ag, Cd)

Voltage	50 kV	Current	Auto
Livetime	100 seconds	Counts Limit	0
Filter	Cu (0.559 mm)	Atmosphere	Vacuum
Maximum Energy	40 keV	Count Rate	High

Low Zb (S, Cl, K, Ca)

Voltage	8 kV	Current	Auto
Livetime	100 seconds	Counts Limit	0
Filter	Cellulose (0.06 mm)	Atmosphere	Vacuum
Maximum Energy	10 keV	Count Rate	Low

[1] Multiple conditions designed to ameliorate peak overlap identified with digital filter background removal, least squares empirical peak deconvolution, gross peak intensities and net peak intensities above background.

[2] Current is set automatically based on the mass absorption coefficient.

Statistical and Graphical Source Assignment.

The data from the WinTrace^{TM} software were translated directly into Excel for Windows software for manipulation and on into SPSS, ver. 21 for Windows and/or JMP 12.01 for statistical analyses as appropriate (Figure 1). IGPET (ver. 2013) is used to create the TAS plots (Figure 2). In order to evaluate these quantitative determinations, machine data were compared to measurements of known standards during each run. RGM-1 a USGS rhyolite (obsidian)

standard is analyzed during each sample run of ≤20 for obsidian artifacts to check machine calibration (Table 1). AGV-1 a USGS andesite standard was run for the non-obsidian volcanic rock analyses (see Table 1).

Source assignments were made by reference to the laboratory data base (see Shackley 1995, 2005, 2011a; Shackley et al. 2016). Further information on the laboratory instrumentation and source data can be found at: http://www.swxrflab.net and (Shackley et al. 2016). Trace element data exhibited here are reported in weight percent (%) and parts per million (ppm), both a quantitative measure by weight, unless otherwise noted.

The elemental concentrations for the artifact data are assigned to source by a stepped statistical and graphical method, outlined in Shackley et al. (2018). Given the dominance of Jemez Lineament sources (i.e. Jemez Mountain and Mount Taylor sources) a Nb versus Y plot is initially used for all obsidian artifacts from all sites (see Figure 1). This effectively discriminates the Jemez Mountains from the Mount Taylor sources (see Shackley et al. 2016). When necessary the high Sr sources are discriminated with a Sr versus Y bivariate plot, or in this case a Sr/Fe plot to discriminate El Rechuelos from Government Mountain. While multivariate statistical analysis (i.e. cluster and discriminant) can be used in these large sample cases, they often assign incorrectly, mainly due to the non-parametric character of compositional analysis leaving empty cells in the sum of squares of cross-products matrix (Baxter 1992, 1994; Glascock 2011; Shackley 1998a). The stepped plotting strategy has been found to be the best approach in Southwestern obsidian provenance studies (Baxter 1992; Shackley 1998; Shackley et al. 2018).

Projectile Point Morphology, Source Provenance and Procurement Range

The Archaic obsidian projectile points from the project were all produced from one of the Jemez Lineament sources in the Jemez Mountains and Mount Taylor Volcanic Field

(Shackley 1998b, 2005; Tables 1 and 2 and cover image here). Some appear to be extensively rejuvenated (DSN # 2110, 2169). Projectile point 2110 would be classified as a Pinto Series point or Gatecliff Split-stemmed on the Colorado Plateau, and point 2169, resembling a Midwest Dalton point rejuvenation appears to be basally ground common in Paleoindian points (see Geib and Jolie 2018; Birkmann et al. 2018; O'Connell and Inoway 1994; Shackley 1989; Thomas 1981; c.f. Chapin 2005; cover image here). Basal grinding on Early Archaic points was seen in the obsidian projectile points from sites in the area, and may indicate that the inhabitants of the sites near Grants, New Mexico just to the south of El Segundo were related or actually the same knappers, particularly given the similar raw material procurement pattern (Birkmann et al. 2018). The production of these points from local and regional obsidian sources is similar between the two nearby areas.

Non-Obsidian Artifacts

The mix of non-obsidian artifacts, mostly volcanics exhibits the same range of rock types as seen in previous studies from El Segundo from ultra-basic rocks to highly siliceous rhyolite and chert (Shackley 2013, 2015b, 2017; Table 3 and Figure 2 here). This assemblage, however, exhibited fewer artifacts produced from rhyolite than in the 2017 study. Whether this was a conscious effort at procurement or sampling error is difficult to know.

Three of the artifacts, two debitage and one projectile point base were produced from dacite. The one point base (DSN 2088) is quite likely produced from the San Antonio Mountain dacite source in the Taos Plateau Volcanic Field (Shackley 2011a, 2013). This is a considerable distance north of the project area (over 250 linear km northeast), but consistent with the procurement distances seen throughout this project, and suggests extensive procurement ranges among these Archaic hunter-gatherers as seen throughout the Southwest (Shackley 1989, 1996, 2005; Vierra 2013).

REFERENCES CITED

Baxter, M.J., 1992, Archaeological uses of the biplot—a neglected technique? In Lock, G., and Moffet J. eds, *Computer Applications and Quantitative Methods in Archaeology*, pp. 141- 148. BAR International Series S577. Oxford, British Archaeological Reports.

Baxter, M.J., 1994, Stepwise discriminant analysis in archaeometry: a critique. *Journal of Archaeological Science* 21:659-666.

Birkmann, J., B.B. Huckell, and M.S. Shackley, 2018, San Jose revisited: the typology, morphometrics, and geochemistry of early Middle Archaic occupation in West-Central, New Mexico. Poster presented at *The Archaic in New Mexico* conference, New Mexico Archaeological Council, Albuquerque, New Mexico, November 10, 2018.

Chapin, N. M., 2005, *Hunter-Gatherer Technological Organization: The Archaic Period in Northern New Mexico*. Ph.D. dissertation, University of New Mexico, Albuquerque.

Davis, M.K., T.L. Jackson, M.S. Shackley, T. Teague, and J. Hampel, 2011, Factors Affecting the Energy-Dispersive X-Ray Fluorescence (EDXRF) Analysis of Archaeological Obsidian. In *X-Ray Fluorescence Spectrometry (XRF) in Geoarchaeology*, edited by M.S. Shackley, pp. 45-64. Springer, New York.

Geib, P.R., and E.A. Jolie, 2018, The rise of broad-spectrum foraging on the Colorado Plateau during the Holocene. In B.J. Vierra (Ed.), *The Archaic Southwest: Foragers in an Arid Land*, pp. 189-214. Salt Lake City: University of Utah Press.

Glascock, M.D., 2011, Comparison and contrast between XRF and NAA: used for characterization of obsidian sources in central Mexico. In Shackley, M.S. (Ed.), *X-Ray Fluorescence Spectrometry (XRF) in Geoarchaeology*, pp. 161-192. New York: Springer.

Govindaraju, K., 1994 , 1994 Compilation of Working Values and Sample Description for 383 Geostandards. *Geostandards Newsletter* 18 (special issue).

Hampel, Joachim H., 1984, Technical Considerations in X-ray Fluorescence Analysis of Obsidian. In *Obsidian Studies in the Great Basin*, edited by R.E. Hughes, pp. 21-25. Contributions of the University of California Archaeological Research Facility 45. Berkeley.

Hildreth, W., 1981, Gradients in Silicic Magma Chambers: Implications for Lithospheric Magmatism. *Journal of Geophysical Research* 86:10153-10192.

Hughes, R. E., and R. L. Smith, 1993, Archaeology, geology, and geochemistry in obsidian provenance studies. *In Scale on Archaeological and Geoscientific Perspectives*, edited by J.K. Stein and A.R. Linse, pp. 79-91. Geological Society of America Special Paper 283.

Mahood, Gail A., and James A. Stimac, 1990, Trace-element partitioning in pantellerites and trachytes. *Geochemica et Cosmochimica Acta* 54:2257-2276.

McCarthy, J.J., and F.H. Schamber, 1981, Least-squares fit with digital filter: a status report. In *Energy Dispersive X-ray Spectrometry*, edited by K.F.J. Heinrich, D.E. Newbury, R.L. Myklebust, and C.E. Fiori, pp. 273-296. National Bureau of Standards Special Publication 604, Washington, D.C.

O'Connell, J.F., and C.M. Inoway, 1994, Surprise Valley projectile points and their chronological implications. *Journal of California and Great Basin Anthropology* 16:162-198.

Schamber, F.H., 1977, A modification of the linear least-squares fitting method which provides continuum suppression. In *X-ray Fluorescence Analysis of Environmental Samples*, edited by T.G. Dzubay, pp. 241-257. Ann Arbor Science Publishers.

Shackley, M.S., 1988, Sources of archaeological obsidian in the Southwest: on archaeological, petrological, and geochemical study. *American Antiquity* 53:752-772.

Shackley, M.S., 1989, *Early Hunter-Gatherer Procurement Ranges in the Southwest: Evidence from Obsidian Geochemistry and Lithic Technology*. Ph.D. dissertation, Arizona State University, Tempe.

Shackley, M. S.,1995, Sources of archaeological obsidian in the greater American Southwest: an update and quantitative analysis. *American Antiquity* 60(3):531-551.

Shackley, M.S., 1996, Range and mobility in the early hunter-gatherer Southwest. In *Early Formative Adaptations in the Southern Southwest*, edited by Barbara Roth, pp. 5-16. Monographs in World Prehistory 25. Prehistory Press, Madison.

Shackley, M.S., 1998a, Current issues and future directions in archaeological volcanic glass studies: an introduction. In M.S. Shackley (Ed.) Archaeological Obsidian Studies: Method and Theory, pp. 1-14. New York: Springer.

Shackley, M.S.,1998b, Geochemical differentiation and prehistoric procurement of obsidian in the Mount Taylor Volcanic Field, Northwest New Mexico. *Journal of Archaeological Science* 25:1073-1082.

Shackley, M.S., 2005, *Obsidian: Geology and Archaeology in the North American Southwest*. University of Arizona Press, Tucson.

Shackley, M.S., 2011a, Sources of archaeological dacite in Northern New Mexico. *Journal of Archaeological Science* 38:1001-1007.

Shackley, M.S., 2011b, An introduction to x-ray fluorescence (XRF) analysis in archaeology. In *X-Ray Fluorescence Spectrometry (XRF) in Geoarchaeology*, M.S. Shackley (Ed.), pp. 7-44. Springer, New York.

Shackley, M.S., 2013, The geochemistry and archaeological petrology of volcanic raw materials in northern New Mexico: obsidian and dacite sources in upland and lowland contects. In B.J. Vierra (Ed.), *From Mountain Top to Valley Bottom: Understanding Past Land Use in the Northern Rio Grande Valley, New Mexico*, pp. 17-32. Salt Lake City: University of Utah Press.

Shackley, M.S., 2015a, Source provenance of obsidian artifacts from the El Segundo archaeology project, Northwestern New Mexico. Report prepared for Southwestern Archaeological Consultants, Santa Fe, New Mexico.

Shackley, M.S., 2015b, Preliminary report of major and minor oxides for volcanic rock artifacts from the El Segundo archaeological project. Report prepared for Southwestern Archaeological Consultants, Santa Fe, New Mexico.

Shackley, M.S., 2016, Source provenance of obsidian artifacts from the El Segundo archaeology project, Northwestern New Mexico. Report prepared for Southwestern Archaeological Consultants, Santa Fe, New Mexico.

Shackley, M.S., 2017, Energy-Dispersive X-Ray Flourescence (EDXRF) Whole Rock Analysis of Major, Minor and Trace Elements for Artifacts from the El Segundo Archaeology Project, Northwestern New Mexico. Report prepared for Southwestern Archaeological Consultants, Santa Fe, New Mexico.

Shackley, M.S., F. Goff, and S.G. Dolan, 2016, Geologic origin of the source of Bearhead Rhyolite (Paliza Canyon) obsidian, Jemez Mountains, northern New Mexico. *New Mexico Geology* 38:52-62.

Shackley, M.S., L.E. Morgan, and D. Pyle, 2018, Elemental, isotopic, and geochronological variability in Mogollon-Datil Volcanic Province archaeological obsidian, southwestern North America: solving issues of inter-source discrimination. *Geoarchaeology* 33:486-497.

Thomas, D.H., 1981, How to classify the projectile points of Monitor Valley, Nevada. *Journal of California and Great Basin Anthropology* 3:7-43.

Vierra, B.J., 2013, Archaic foraging technology and land use in the northern Rio Grande, New Mexico. In B.J. Vierra (Ed.), *From Mountain Top to Valley Bottom: Understanding Past Land Use in the Northern Rio Grande Valley, New Mexico*, pp. 145-160. Salt Lake City: University of Utah Press.

Table 1. Elemental concentrations for the obsidian artifacts, and USGS RGM-1 rhyolite standard. All measurements in parts per million (ppm).

Sample	Site	Ti	Mn	Fe	Rb	Sr	Y	Zr	Nb	Ba	Pb	Th	Source
2162	IO	668	438	9059	163	14	47	167	58		21	19	Valles Rhy (Cerro del Medio)
2163	IO	658	430	9339	168	16	44	177	54		23	21	Valles Rhy (Cerro del Medio)
2164	IO	634	358	8108	149	15	39	163	52		22	24	Valles Rhy (Cerro del Medio)
2165	IO	614	392	8629	157	13	45	166	63		23	26	Valles Rhy (Cerro del Medio)
2166	IO	904	403	10076	155	15	44	167	51		24	19	Valles Rhy (Cerro del Medio)
2167	IO	741	406	9262	163	13	44	174	57		26	21	Valles Rhy (Cerro del Medio)
2168	IO	669	393	8852	162	14	48	167	54		24	20	Valles Rhy (Cerro del Medio)
2169	IO	1039	419	11270	166	15	45	173	55		28	23	Valles Rhy (Cerro del Medio)
2170	IO	628	422	9130	164	9	42	176	59		23	17	Valles Rhy (Cerro del Medio)
2171	IO	613	419	5418	148	14	21	74	46		26	25	El Rechuelos Rhyolite
2172	IO	619	430	5449	155	14	22	79	50		23	24	El Rechuelos Rhyolite
2173	IO	624	403	5076	143	13	24	72	49		20	18	El Rechuelos Rhyolite
2174	IO	504	671	7257	540	16	78	120	191		50	19	Grants Ridge, Mt Taylor
2175	IO	416	723	7329	565	12	78	119	196		63	31	Grants Ridge, Mt Taylor
2176	IO	409	679	6872	548	13	76	119	194		60	34	Grants Ridge, Mt Taylor
2177	IO	514	603	8984	518	12	91	143	225		57	30	Horace/La Jara Mesa, Mt Taylor
2178	IO	391	531	8060	498	14	89	140	231		54	20	Horace/La Jara Mesa, Mt Taylor
2179	IO	429	472	7555	456	15	86	133	214		46	35	Horace/La Jara Mesa, Mt Taylor
2180	IO	478	551	8276	492	11	92	139	233		52	31	Horace/La Jara Mesa, Mt Taylor
2181	IO	395	515	7885	492	13	84	133	221		47	30	Horace/La Jara Mesa, Mt Taylor
2182	IO	465	657	10239	569	14	98	149	241		61	35	Horace/La Jara Mesa, Mt Taylor
2183	IO	415	561	8358	511	12	89	139	234		57	35	Horace/La Jara Mesa, Mt Taylor
2105	LA 27848	695	398	8969	161	13	45	170	59		25	17	Valles Rhy (Cerro del Medio)
2106	LA 27848	1058	551	12785	193	13	49	176	56		32	26	Valles Rhy (Cerro del Medio)
2107	LA 27848	392	606	8789	552	14	94	147	232		63	31	Horace/La Jara Mesa, Mt Taylor
2108	LA 27848	411	710	7086	558	10	77	122	193		58	25	Grants Ridge, Mt Taylor
2109	LA 27848	366	712	6931	548	12	83	119	188		60	29	Grants Ridge, Mt Taylor

Sample	Site	Ti	Mn	Fe	Rb	Sr	Y	Zr	Nb	Ba	Pb	Th	Source
2110	LA 137164	573	367	8141	156	10	48	161	50		26	25	Valles Rhy (Cerro del Medio)
2111	LA 137164	834	417	10113	168	15	46	164	59		30	28	Valles Rhy (Cerro del Medio)
2112	LA 137164	616	452	8615	205	13	64	172	91		35	35	Cerro Toledo Rhy
2113	LA 137164	632	489	9313	213	14	65	183	97		33	30	Cerro Toledo Rhy
2114	LA 137164	949	505	12871	206	14	50	188	63		31	34	Valles Rhy (Cerro del Medio)
2115	LA 137164	467	505	9081	211	11	63	181	96		34	27	Cerro Toledo Rhy
2116	LA 137164	466	838	8145	577	12	86	118	200		60	31	Grants Ridge, Mt Taylor
1996	LA 149563	779	561	10145	519	13	87	143	238		50	30	Horace/La Jara Mesa, Mt Taylor
1997	LA 149563	854	462	10415	205	9	63	180	103		33	31	Cerro Toledo Rhy
1998	LA 165742	687	389	8657	154	11	46	164	52		24	23	Valles Rhy (Cerro del Medio)
1999	LA 165742	552	494	9536	218	11	66	181	97		31	23	Cerro Toledo Rhy
2100	LA 165742	744	390	5278	155	13	26	73	48		26	14	El Rechuelos Rhyolite
2101	LA 165742	646	409	9204	168	16	49	169	57		23	22	Valles Rhy (Cerro del Medio)
2102	LA 165742	405	737	10405	614	16	102	151	246		70	30	Horace/La Jara Mesa, Mt Taylor
2103	LA 165742	796	450	6166	166	15	20	71	48		27	19	El Rechuelos Rhyolite
2104	LA 165742	451	851	7880	609	12	78	119	194		70	39	Grants Ridge, Mt Taylor
2117	LA 27799/27800	441	542	8594	113	81	19	81	57	348	38	24	Government Mtn
2118	LA 27799/27800	351	733	6967	551	13	82	117	184		62	29	Grants Ridge, Mt Taylor
2119	LA 27799/27800	438	792	7653	566	9	84	117	185		68	30	Grants Ridge, Mt Taylor
2120	LA 27799/27800	456	740	7361	578	14	74	118	193		61	32	Grants Ridge, Mt Taylor
2121	LA 27799/27800	386	738	7273	576	11	72	120	187		65	31	Grants Ridge, Mt Taylor
2122	LA 27799/27800	622	994	7842	544	12	83	117	197		62	36	Grants Ridge, Mt Taylor
2123	LA 27799/27800	504	675	6797	530	9	81	115	191		60	29	Grants Ridge, Mt Taylor
2124	LA 27799/27800	486	744	7498	562	11	84	119	197		68	35	Grants Ridge, Mt Taylor
2125	LA 27799/27800	434	853	11381	477	14	88	136	216		56	32	Horace/La Jara Mesa, Mt Taylor
2126	LA 27799/27800	416	559	8521	522	11	94	141	225		58	35	Horace/La Jara Mesa, Mt Taylor
2127	LA 27799/27800	673	515	10270	224	12	68	184	94		43	27	Cerro Toledo Rhy
2128	LA 27799/27800	694	533	9670	224	13	65	175	101		34	18	Cerro Toledo Rhy
2129	LA 27799/27800	294	566	8172	518	13	89	141	218		53	28	Horace/La Jara Mesa, Mt Taylor
2130	LA 27799/27800	610	472	9254	199	10	60	178	98		36	29	Cerro Toledo Rhy
2131	LA 27799/27800	405	581	8864	519	12	96	146	226		62	29	Horace/La Jara Mesa, Mt Taylor

2132	LA 27799/27800	537	458	8916	207	10	62	178	96		36	33	Cerro Toledo Rhy
2133	LA 27799/27800	609	491	9333	203	12	65	179	88		35	31	Cerro Toledo Rhy
2134	LA 27799/27800	630	499	9358	206	13	65	176	92		38	24	Cerro Toledo Rhy
2135	LA 27799/27800	582	627	9350	523	16	98	144	227		55	39	Horace/La Jara Mesa, Mt Taylor
2136	LA 27799/27800	702	586	11247	233	9	69	194	101		43	27	Cerro Toledo Rhy
2137	LA 27799/27800	732	422	5631	158	13	24	75	45		23	20	El Rechuelos Rhyolite
2138	LA 27799/27800	725	420	5666	158	13	29	73	46		30	26	El Rechuelos Rhyolite
2139	LA 27799/27800	684	367	8758	165	10	45	167	56		27	29	Valles Rhy (Cerro del Medio)
2140	LA 27799/27800	769	434	10425	173	17	44	176	53		32	30	Valles Rhy (Cerro del Medio)
2141	LA 27799/27800	589	592	10675	236	12	65	187	104		41	29	Cerro Toledo Rhy
Sample	Site	Ti	Mn	Fe	Rb	Sr	Y	Zr	Nb	Ba	Pb	Th	Source
2142	LA 27799/27800	740	399	8927	174	13	40	167	57		22	16	Valles Rhy (Cerro del Medio)
2143	LA 27799/27800	558	563	10448	220	12	62	175	107		45	27	Cerro Toledo Rhy
2144	LA 27799/27800	747	438	9873	168	16	42	178	61		27	31	Valles Rhy (Cerro del Medio)
2145	LA 27799/27800	769	390	9095	162	14	45	164	58		24	18	Valles Rhy (Cerro del Medio)
2146	LA 27799/27800	604	385	9203	185	15	44	168	55		46	28	Valles Rhy (Cerro del Medio)
2147	LA 27799/27800	777	408	9298	164	12	45	163	57		29	28	Valles Rhy (Cerro del Medio)
2148	LA 27799/27800	764	707	8834	158	13	47	162	57		24	21	Valles Rhy (Cerro del Medio)
2149	LA 27799/27800	571	397	8350	150	10	42	169	52		25	27	Valles Rhy (Cerro del Medio)
2150	LA 27799/27800	505	469	8729	198	9	61	179	95		37	30	Cerro Toledo Rhy
2151	LA 27799/27800	706	418	9229	168	11	45	174	46		29	27	Valles Rhy (Cerro del Medio)
2152	LA 27799/27800	765	589	10975	241	10	70	190	95		42	24	Cerro Toledo Rhy
2153	LA 27799/27800	718	542	10352	223	10	70	182	97		40	33	Cerro Toledo Rhy
2154	LA 27799/27800	630	561	10271	221	14	70	180	107		32	33	Cerro Toledo Rhy
2155	LA 27799/27800	637	544	10211	216	10	68	183	107		41	35	Cerro Toledo Rhy
2156	LA 27799/27800	617	525	9573	213	11	67	176	98		36	33	Cerro Toledo Rhy
2157	LA 27799/27800	932	541	11349	226	13	70	187	97		47	23	Cerro Toledo Rhy
2158	LA 27799/27800	719	638	9171	156	13	46	169	50		27	31	Valles Rhy (Cerro del Medio)
2159	LA 27799/27800	584	483	9589	211	9	70	180	92		34	16	Cerro Toledo Rhy
2160	LA 27799/27800	606	413	9269	167	19	44	165	54		25	27	Valles Rhy (Cerro del Medio)
2161	LA 27799/27800	735	469	8588	153	13	42	174	57		21	31	Valles Rhy (Cerro del Medio)
RGM1-S4		1478	319	13077	150	111	22	219	8		20	15	standard
RGM1-S4		1469	296	13047	151	100	24	222	11		19	16	standard
RGM1-S4		1508	305	13044	150	110	24	220	11		20	16	standard
RGM1-S6		1423	336	13173	148	110	31	218	7		22	19	standard
RGM1-S6		1501	315	13042	147	105	18	218	6		23	17	standard

RGM1-S4	1561	302	13206	149	109	31	220	8	835	24	22	standard

Table 2. Crosstabulation of obsidian source by site/isolate points.

			Source						
			Valles Rhy (Cerro del Medio)	Cerro Toledo Rhy	El Rechuelos Rhyolite	Horace/La Jara Mesa, Mt Taylor	Grants Ridge, Mt Taylor	Government Mtn	Total
Site	Isolated Proj Points	Count	9	0	3	7	3	0	22
		% within Site	40.9%	0.0%	13.6%	31.8%	13.6%	0.0%	100.0%
		% within Source	31.0%	0.0%	42.9%	46.7%	21.4%	0.0%	25.0%
		% of Total	10.2%	0.0%	3.4%	8.0%	3.4%	0.0%	25.0%
	LA 137164	Count	3	3	0	0	1	0	7
		% within Site	42.9%	42.9%	0.0%	0.0%	14.3%	0.0%	100.0%
		% within Source	10.3%	13.6%	0.0%	0.0%	7.1%	0.0%	8.0%
		% of Total	3.4%	3.4%	0.0%	0.0%	1.1%	0.0%	8.0%
	LA 149563	Count	0	1	0	1	0	0	2
		% within Site	0.0%	50.0%	0.0%	50.0%	0.0%	0.0%	100.0%
		% within Source	0.0%	4.5%	0.0%	6.7%	0.0%	0.0%	2.3%
		% of Total	0.0%	1.1%	0.0%	1.1%	0.0%	0.0%	2.3%
	LA 165742	Count	2	1	2	1	1	0	7
		% within Site	28.6%	14.3%	28.6%	14.3%	14.3%	0.0%	100.0%
		% within Source	6.9%	4.5%	28.6%	6.7%	7.1%	0.0%	8.0%
		% of Total	2.3%	1.1%	2.3%	1.1%	1.1%	0.0%	8.0%
	LA 27799/27800	Count	13	17	2	5	7	1	45
		% within Site	28.9%	37.8%	4.4%	11.1%	15.6%	2.2%	100.0%
		% within Source	44.8%	77.3%	28.6%	33.3%	50.0%	100.0%	51.1%
		% of Total	14.8%	19.3%	2.3%	5.7%	8.0%	1.1%	51.1%
	LA 27848	Count	2	0	0	1	2	0	5
		% within Site	40.0%	0.0%	0.0%	20.0%	40.0%	0.0%	100.0%
		% within Source	6.9%	0.0%	0.0%	6.7%	14.3%	0.0%	5.7%
		% of Total	2.3%	0.0%	0.0%	1.1%	2.3%	0.0%	5.7%
Total		Count	29	22	7	15	14	1	88
		% within Site	33.0%	25.0%	8.0%	17.0%	15.9%	1.1%	100.0%
		% within Source	100.0%	100.0%	100.0%	100.0%	100.0%	100.0%	100.0%
		% of Total	33.0%	25.0%	8.0%	17.0%	15.9%	1.1%	100.0%

Table 3. Major, minor and trace element concentrations for the non-obsidian artifacts, and USGS AGV-1 andesite standard. Measurements in weight percent or parts per million (ppm) as noted.

DSN	Na2O %	MgO %	Al2O3 %	SiO2 %	P2O5 %	K2O %	CaO %	TiO2 %	V2O5 %	Cr2O3 %	MnO %	Fe2O3 %	As2O5 %	Σ	Rock Type
2068	3.0	1.3	11.0	48.6	0.6	4.0	11.9	1.9	0.1	0.1	0.3	16.7	0.0	99.4	basaltic trachy-andesite
2069	2.3	0.4	10.7	56.6	0.3	5.9	8.3	1.3	0.1	0.0	0.2	12.9	0.0	99.1	trachy-andesite
2070	2.8	0.8	11.6	40.1	1.1	2.6	11.6	5.7	0.2	0.0	0.3	22.1	0.0	98.9	tephrite
2071	3.1	0.2	11.9	56.9	0.5	5.9	7.8	1.7	0.1	0.0	0.2	10.4	0.0	98.7	trachy-andesite
2072	3.0	0.9	14.1	75.2	0.0	4.2	0.5	0.3	0.0	0.0	0.0	1.5	0.0	99.6	rhyolite
2073	3.1	0.6	7.4	69.8	0.7	3.5	8.8	2.8	0.1	0.0	0.1	3.0	0.0	99.6	dacite
2074	1.0	1.8	25.9	47.8	0.2	2.1	2.6	2.7	0.1	0.0	0.1	12.6	0.0	97.0	basalt
2075	1.4	2.2	6.8	17.2	0.3	0.7	0.8	0.0	0.0	0.0	6.2	64.0	0.0	99.6	not volcanic
2076	2.9	1.1	11.1	48.6	0.4	3.8	12.3	1.9	0.1	0.0	0.3	17.0	0.0	99.6	basaltic trachy-andesite
2077	2.6	0.9	11.2	48.9	0.5	4.2	11.6	2.0	0.1	0.0	0.3	17.2	0.0	99.6	trachy-basalt
2078	3.3	1.4	10.7	46.7	0.5	3.6	13.4	1.7	0.1	0.1	0.3	17.8	0.0	99.5	tephrite
2079	2.8	1.5	10.5	42.1	0.6	2.3	14.6	2.1	0.2	0.1	0.5	22.3	0.0	99.3	tephrite
2080	2.6	1.4	8.4	35.3	0.9	3.8	10.6	7.4	0.3	0.0	0.4	27.5	0.0	98.6	nephelinite
2081	4.2	1.8	6.9	30.6	0.9	3.8	10.8	8.3	0.3	0.0	0.5	30.9	0.0	98.9	nephelinite
2082	2.3	2.1	6.9	30.4	0.8	3.6	11.0	8.1	0.2	0.0	0.5	32.6	0.0	98.4	nephelinite
2083	2.9	6.8	14.7	50.2	0.2	0.4	9.9	1.2	0.1	0.0	0.2	13.1	0.0	99.7	basalt
2084	3.3	2.9	19.1	58.7	0.0	2.1	5.8	0.9	0.0	0.0	0.1	6.9	0.0	99.8	andesite
2085	3.6	0.7	10.4	47.5	0.8	3.9	13.0	1.8	0.1	0.1	0.3	17.3	0.0	99.5	tephrite
2086	2.0	1.6	18.2	67.1	0.0	3.1	0.9	0.9	0.0	0.0	0.0	5.2	0.0	99.1	dacite
2087	1.5	3.1	22.0	61.4	0.0	2.9	1.2	0.9	0.1	0.0	0.1	6.3	0.0	99.4	andesite
2088	4.2	1.7	17.0	64.9	0.0	2.7	3.8	0.6	0.0	0.0	0.1	4.4	0.0	99.6	San Antonio Mtn dacite
2089	2.0	0.1	0.4	92.1	0.0	0.2	0.5	0.0	0.0	0.0	3.7	0.2	0.0	99.3	chert?
AGV1-S1	4.0	0.6	16.7	62.2	0.0	3.1	5.1	1.0	0.0	0.0	0.1	6.8	0.0	99.7	
USGS Rec.	4.3	1.5	17.2	58.8	0.5	2.9	4.9	1.1	nr	nr	nr	6.8	nr		

DSN	Zn ppm	Ga ppm	Rb ppm	Sr ppm	Zr ppm	Nb ppm	Ba ppm	Pb ppm	Th ppm
2068	102	16	73	235	111	22	367	16	13
2069	100	18	68	584	272	24	1775	16	20

2070	145	20	26	969	261	48	2743	4	13
2071	92	17	72	608	202	33	1445	16	9
DSN	Zn	Ga	Rb	Sr	Zr	Nb	Ba	Pb	Th
2072	34	15	125	90	233	12	2063	48	19
2073	93	18	90	96	219	24	337	19	15
2074	171	22	31	1383	472	99	1623	17	4
2075	118	8	78	433	47	4	591	11	4
2076	96	20	71	227	107	27	401	13	4
2077	87	18	74	232	108	15	399	14	9
2078	96	20	75	225	104	27	405	19	4
2079	96	20	62	253	111	21	399	11	4
2080	220	18	64	1135	428	97	2820	13	4
2081	293	20	58	1206	433	86	2443	16	4
2082	214	26	54	1271	484	96	1668	5	6
2083	123	17	6	219	93	4	154	-1	4
2084	68	17	60	229	109	19	386	16	12
2085	128	18	78	232	103	18	351	22	4
2086	133	17	90	131	166	15	602	17	20
2087	250	22	148	247	196	24	847	25	18
2088	70	19	54	538	206	38	2030	20	16
2089	16	10	0	105	16	4	2088	7	4
AGV1-S1	81	22	68	649	233	11	1223	29	7
USGS Rec.	88	20	67	660	227	15	1230	36	7

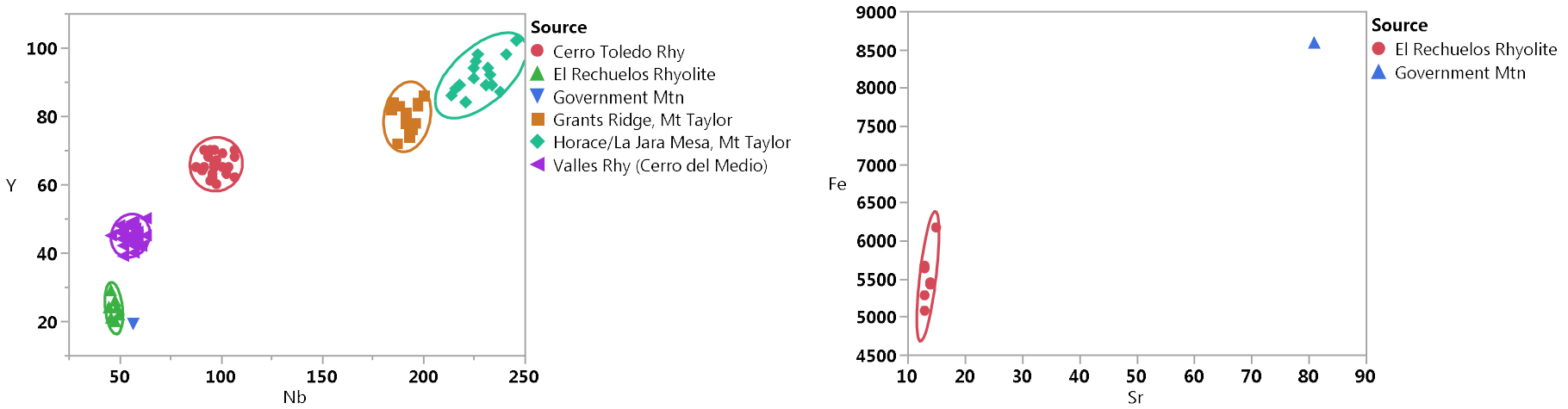

Figure 1. Nb/Y bivariate plot of all the obsidian artifacts (left), and Sr/Fe bivariate plot of El Rechuelos and Government Mountain samples (right) to provide better discrimination. Confidence ellipses at 95%.

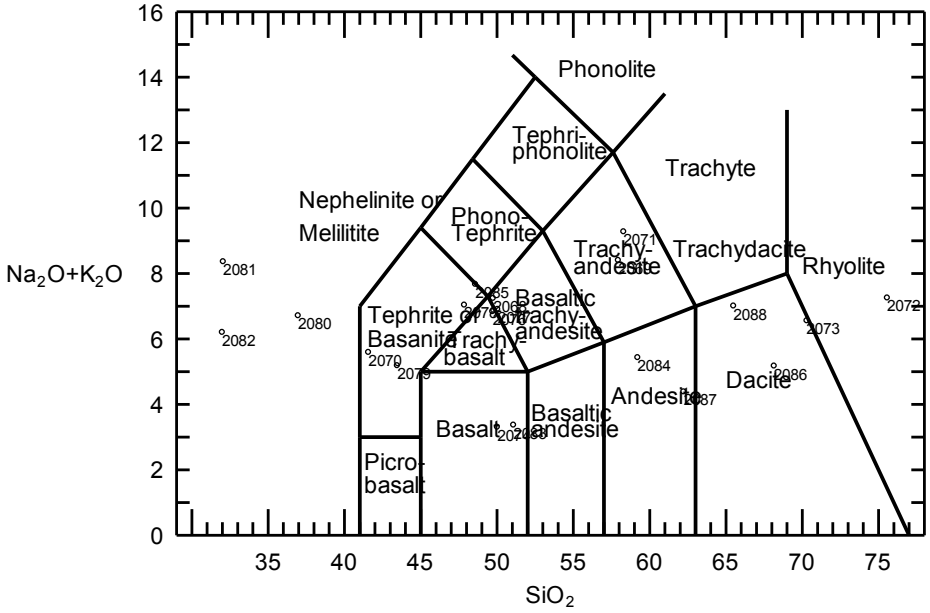

Figure 2. TAS plot of the volcanic rock artifacts. The chert rock sample removed (see Table 3). AGV-1, a high alkali andesite, plots slightly high on silica, but basically correct on the alkalis.